Implications of MAVEN's planetographic coordinate system for comparisons to other recent Mars orbital missions

Paul Withers[1,2] and B. M. Jakosky[3]

[1]Department of Astronomy, Boston University, USA.

[2]Center for Space Physics, Boston University, USA.

[3]Laboratory for Atmospheric and Space Physics, University of Colorado, USA.

This article has been accepted for publication and undergone full peer review but has not been through the copyediting, typesetting, pagination and proofreading process, which may lead to differences between this version and the Version of Record. Please cite this article as doi: 10.1002/2016JA023470

Abstract. MAVEN uses a planetographic coordinate system to report altitude, latitude, and longitude on Mars. By contrast, Mars Global Surveyor, Mars Odyssey, Mars Express, and Mars Reconnaissance Orbiter generally used a planetocentric coordinate system. These two coordinate systems are different: latitudes differ by up to 0.34 degrees and altitudes differ by up to 2 km. These differences are large enough to affect the scientific results of comparisons between MAVEN and other orbital datasets. This is illustrated with three examples. (A) Comparisons of neutral density inferred from ionospheric peak altitude could contain errors of 25%. (B) Comparisons of mesopause altitude found from ultraviolet stellar occultations could contain errors of 2 km. (C) Comparisons of zonal variations in thermospheric density found from accelerometer observations could contain errors of 12%. Scientists who compare MAVEN data to other datasets, or to models derived from other datasets, should be aware of these differences in the coordinate systems and make appropriate adjustments.

1. Introduction

The time and position of a spacecraft observation are critically important for interpretation of the observation. This imposes a requirement for precise and unambiguous definition of coordinate systems. Several different coordinate systems have been used for Mars observations since the first spacecraft missions to that planet. Two classes of planet-fixed coordinate system have been widely used: planetographic and planetocentric. These two coordinate systems adopt different definitions of terms as fundamental as "altitude" and "latitude". MAVEN generally uses a planetographic coordinate system to describe planet-fixed altitude and latitude, in contrast to many recent Mars orbital missions that have used a planetocentric coordinate system. Here we quantify differences in altitude and latitude between the two coordinate systems (Section 2). We also discuss several examples of potential comparisons between MAVEN datasets and datasets from other missions (Section 3). These examples illustrate that differences between the two coordinate systems will negatively impact the scientific results derived from such comparisons if these differences are not accounted for properly.

2. Planetographic and planetocentric coordinate systems at Mars

Figure **??** illustrates the planetographic and planetocentric coordinate systems, highlighting their different definitions of latitude and altitude.

The Mariner and Viking missions generally adopted a planetographic coordinate system. The origin is the center of mass. The north pole (+90° latitude) is defined as the rotational pole on the north side of the invariable plane of the solar system. Note that this definition is independent of the direction of Mars's rotation. From the north pole, the equator

(0° latitude) and south pole (-90° latitude) follow straightforwardly. Latitudes of other locations are defined relative to a reference ellipsoid of rotation. The current reference ellipsoid [*Archinal et al.*, 2011] has a polar radius, r_p, of 3376.20 km and an equatorial radius, r_e, of 3396.19 km. These radii differ by 20 km and correspond to a flattening f of $(r_e - r_p)/r_e = 5.9 \times 10^{-3}$. The magnitude of the planetographic latitude of a point on the reference ellipsoid is defined as the angle between the normal to the reference ellipsoid at that point and the equatorial plane. Latitudes are positive in the northern hemisphere, negative in the southern hemisphere. The planetographic latitude of a point not on the reference ellipsoid is the planetographic latitude of the closest point on the reference ellipsoid. This is equivalent to rescaling the radii of the reference ellipsoid by a common factor such that the point now lies on the rescaled reference ellipsoid. The planetographic altitude of a point is defined as the separation between that point and the closest point on the reference ellipsoid. The planetographic longitude of a point is defined as the angle between two half-planes. The first half-plane is the meridional plane that contains the point and the second half-plane is the meridional plane that contains the reference point for the prime meridian.

After much debate, the Mars Global Surveyor (MGS) mission generally adopted a planetocentric coordinate system. The Mars Odyssey (ODY), Mars Express (MEX), and Mars Reconnaissance Orbiter (MRO) missions followed the same conventions as Mars Global Surveyor. In a planetocentric coordinate system, the origin, poles, and equator are as in a planetographic system, but planetocentric latitude and longitude are as in the spherical polar coordinate system commonly used in mathematics. Longitude is essentially the same in the two systems [*Archinal et al.*, 2011]. In a planeto-

centric coordinate system, the altitude of a point is defined as the separation between that point and the point with the same latitude and longitude on a reference surface. The reference surface is usually an equipotential surface known as the "MOLA areoid" [http://geo.pds.nasa.gov/missions/mgs/megdr.html, *Archinal et al.*, 2011]. This is based on data from the Mars Orbiter Laser Altimeter (MOLA) instrument. The radial distance to the reference surface depends on latitude and longitude. Unlike the planetographic reference ellipsoid, it is not rotationally symmetric.

Planetographic and planetocentric latitudes are related. The equation of an ellipse is:

$$\left(\frac{x}{a}\right)^2 + \left(\frac{y}{b}\right)^2 = 1 \tag{1}$$

The gradient dy/dx satisfies:

$$\frac{dy}{dx} = -\left(\frac{x}{y}\right)\left(\frac{b^2}{a^2}\right) \tag{2}$$

Figure **??**A shows a point (x, y) on the surface of the reference ellipsoid. Its latitude is defined in terms of its relationship to the point $(p, 0)$. In order for the line from $(p, 0)$ to (x, y) to be perpendicular to the perimeter of the ellipse, the following condition must be satisfied:

$$\frac{y-0}{x-p} = -\frac{dx}{dy} = \left(\frac{y}{x}\right)\left(\frac{a^2}{b^2}\right) \tag{3}$$

The planetographic latitude θ_g satisfies $\tan\theta_g = (y-0)\,/\,(x-p)$ and the planetocentric latitude θ_c satisfies $\tan\theta_c = y/x$. Hence:

$$\tan\theta_g = \left(\frac{a^2}{b^2}\right)\tan\theta_c \tag{4}$$

Since the flattening f equals $(a-b)/a$,

$$\tan\theta_c = (1-f)^2\tan\theta_g \tag{5}$$

Equation 5 can be used to convert planetographic and planetocentric latitudes. It is exact for points on the reference ellipsoid. Note, however, that the line through point (x, y) that defines the point's planetocentric latitude is not parallel to the line through point (x, y) that defines the point's planetographic latitude. Consequently, Equation 5 is not exactly satisfied for points off the reference ellipsoid. It is, however, a reasonable approximation for points close enough to the reference ellipsoid that their altitudes are much less than the planetary radius. That condition is satisfied for the crust, surface, atmosphere, and ionosphere, but not the magnetosphere.

Figure 2A shows the difference $\delta = \theta_g - \theta_c$ as a function of θ_c. It follows from Equation 5 and the assumption that $f \ll 1$ that δ satisfies $\delta = f\sin(2\theta_c)$. Hence the greatest difference between the two latitudes is f radians or $180f/\pi$ degrees, which is 0.34 degrees. This occurs at $\theta_c = 45°$.

Figure 3A shows the radius of the planetographic reference ellipsoid, r_g, as a function of *planetocentric* latitude and longitude. From Equation 1, r_g satisfies:

$$r_g^2 = \frac{a^2(1-f)^2(1+\tan^2\theta_c)}{(1-f)^2+\tan^2\theta_c} \tag{6}$$

Similarly, Figure 3B shows the radius of the planetocentric reference surface as a function of planetocentric latitude and longitude. The gross shape of the planetocentric reference surface matches the longitude-independent planetographic reference ellipsoid, but differences are apparent. These are most noticeable around the Tharsis region.

Figure 3C shows the difference between planetographic altitude and planetocentric altitude as a function of planetocentric latitude and longitude. Figure 2B shows the difference between planetographic altitude and planetocentric altitude as a function of planetocentric latitude. The difference is broadly symmetric about the equator. Planetocentric altitude is 2 km less than planetographic altitude near the poles, and is always less than planetographic altitude when latitude is poleward of 30° latitude. Equatorward of 30° latitude, the sign of the difference varies, but the magnitude of the difference is generally less than 1 km. However, planetocentric altitude is smaller than planetographic altitude by 1 km or more near Olympus Mons and the three Tharsis Montes.

3. MAVEN

Some MAVEN data products at the NASA Planetary Data System (PDS), particularly those generated by the Particles and Fields suite, report position in a Cartesian coordinate system that does not explicitly use altitude or latitude. Other MAVEN PDS data products generally use the planetographic coordinate system outlined above when specifying altitude, latitude, or longitude. The coordinate system is explicitly defined in the accompanying documentation. However, not all publications that use MAVEN PDS data products note that latitudes and altitudes are expressed in the planetographic coordinate system. Nor do all publications that use MGS, ODY, MEX, or MRO PDS data products note that latitudes and altitudes are expressed in the planetocentric coordinate system.

Furthermore, it should be noted that the MAVEN Key Parameter data products define altitude with respect to the MOLA areoid.

For atmospheric or surface studies, differences in the local gravitational potential between two locations are important. That favors a definition of altitude relative to an equipotential surface, such as the MOLA areoid used in the planetocentric system. For MAVEN, however, transformations between solar-fixed (e.g., Mars-centered solar orbital, MSO) and planet-fixed coordinates are important. Solar-fixed coordinates are most appropriate for descriptions of the magnetosphere, whereas effects of crustal magnetic fields require planet-fixed coordinates. That favors a planet-fixed coordinate system that is readily transformed into a solar-fixed coordinate system, such as the ellipsoid-based planetographic system.

Comparison of MAVEN data products and derived empirical models to MGS, ODY, MEX, and MRO data products and derived empirical models should consider the consequences of differences in the underlying coordinate systems. Three examples of possible comparisons are: (A) Comparison of MAVEN ionospheric densities and previous radio occultation ionospheric densities, (B) Comparison of MAVEN and MEX stellar occultation profiles of atmospheric temperatures, and (C) Comparison of MAVEN and MGS accelerometer measurements of zonal variations in thermospheric densities. Next we show that differences in coordinate systems can significantly impact the scientific results of such comparisons.

3.1. Comparison of MAVEN ionospheric densities and previous radio occultation ionospheric densities

The MGS radio occultation experiment acquired 5600 ionospheric electron density profiles, an order of magnitude more than any other radio occultation experiment [*Mendillo et al.*, 2003; *Withers et al.*, 2008]. The MAVEN Langmuir probe (LPW) [*Andersson et al.*, 2015] and ion mass spectrometer (NGIMS) [*Mahaffy et al.*, 2015] make in situ measurements of ionospheric plasma densities that sometimes extend low enough to measure densities at the main peak of the ionosphere [Vogt et al., this issue].

Analysis of MGS and other pre-MAVEN observations has shown that the altitude of the main peak of the ionosphere, Z_m, varies with solar zenith angle χ as $Z_m = Z_0 + L \ln \sec \chi$, where Z_0 is approximately 120 km and L is approximately 10 km [*Fallows et al.*, 2015, and references therein]. The implied subsolar peak altitude Z_0 is the altitude at which the vertical optical depth, $\sigma n H$, equals 1. Here σ is an ionization cross-section, n is the neutral number density, and H is the neutral scale height, which is on the order of 8 km [*Withers*, 2006]. Fitted values of Z_0 from MAVEN at one season and latitude could be compared to fitted values of Z_0 from MGS at the same season and latitude in order to investigate interannual variability in thermospheric conditions, or could be compared to fitted values at the same season and different latitude in order to investigate thermospheric gradients with latitude. Since the altitude of a given location on Mars can differ by 2 km between the two coordinate systems, the inferred neutral number density could be in error by 25% for a scale height of 8 km. Worse, the resultant error would have a systematic dependence on latitude.

3.2. Comparison of MAVEN and MEX stellar occultation profiles of atmospheric temperatures

The MEX SPICAM instrument has measured many vertical profiles of atmospheric temperature between 60 and 130 km using ultraviolet observations of stellar occultations [*Forget et al.*, 2009; *Withers et al.*, 2011]. The MAVEN IUVS instrument makes similar measurements [*McClintock et al.*, 2015]. One of the most prominent features of such temperature profiles is the mesopause, which is a temperature minimum around 100 km. Mesopause temperatures can drop below 100 K, cold enough to form CO_2 clouds [*Magalhães et al.*, 1999; *Montmessin et al.*, 2006; *Forget et al.*, 2009; *Holstein-Rathlou et al.*, 2016]. The mesopause plays a key role in the energy balance of the atmosphere [*Chamberlain and Hunten*, 1987]. It is the boundary between the radiatively-controlled middle atmosphere and the conductively-controlled thermosphere. The mesopause altitude varies with season, solar cycle, and other factors. For reference, the mesopause altitudes in Pathfinder and Curiosity entry temperature profiles differ by 4 km [*Magalhães et al.*, 1999; *Holstein-Rathlou et al.*, 2016]. The mesopause altitude in MEX and MAVEN temperature profiles could be compared in order to investigate the effects of the solar cycle or seasons on the thermal structure of the atmosphere. Erroneous results could be generated if the 2 km altitude difference between the two coordinate systems is not properly accounted for.

3.3. Comparison of MAVEN and MGS accelerometer measurements of atmospheric density variations caused by thermal tides

The MGS accelerometer instrument measured variations in thermospheric density with longitude and interpreted them as being caused by thermal tides [e.g., *Withers et al.*, 2003]. The MAVEN accelerometer instrument makes similar measurements [*Zurek et al.*,

2015]. Other MAVEN instruments can also be used to study atmospheric thermal tides [*Lo et al.*, 2015; *England et al.*, 2016]. Figure 3C shows that the difference between planetographic altitude and planetocentric altitude in the tropics has a striking wave-2 dependence on longitude with an amplitude of ±1 km. Given a density scale height of 8 km at 130 km [*Withers*, 2006], atmospheric densities that show no variation on longitude in one coordinate system will show a wave-2 variation with longitude with an amplitude of 12% in the other coordinate system. Erroneous scientific conclusions could be reached if this effect is not properly accounted for.

4. Summary

Differences exist between the planet-fixed coordinate systems used by MAVEN and other recent Mars orbital missions. Their definitions of altitude and latitude are different. These differences are large enough that they should be considered when datasets or models are compared between missions.

The JPL NAIF SPICE system provides excellent tools to convert between many different coordinate systems, including tools to convert planetocentric radial distance, latitude, and longitude into planetographic altitude, latitude, and longitude, but it does not include a conversion from planetocentric radial distance to planetocentric altitude related to the MOLA areoid. A suitable planetocentric coordinate system that includes altitudes referenced to the MOLA areoid would be a valuable addition to SPICE.

Acknowledgments. PW was supported, in part, by NASA award NNX13AO35G. MAVEN data are available from the NASA Planetary Data System (http://pds.nasa.gov). The MAVEN project is supported by NASA through the Mars Exploration Program.

References

Acuna, M. H., J. E. P. Connerney, N. F. Ness, R. P. Lin, D. Mitchell, C. W. Carlson, J. McFadden, K. A. Anderson, H. Reme, C. Mazelle, D. Vignes, P. Wasilewski, and P. Cloutier (1999), Global distribution of crustal magnetization discovered by the Mars Global Surveyor MAG/ER experiment, *Science*, *284*, 790, doi:10.1126/science.284.5415.790.

Andersson, L., R. E. Ergun, G. T. Delory, A. Eriksson, J. Westfall, H. Reed, J. McCauly, D. Summers, and D. Meyers (2015), The Langmuir Probe and Waves (LPW) instrument for MAVEN, *Space Sci. Rev.*, *195*, 173–198, doi:10.1007/s11214-015-0194-3.

Archinal, B. A., M. F. A'Hearn, E. Bowell, A. Conrad, G. J. Consolmagno, R. Courtin, T. Fukushima, D. Hestroffer, J. L. Hilton, G. A. Krasinsky, G. Neumann, J. Oberst, P. K. Seidelmann, P. Stooke, D. J. Tholen, P. C. Thomas, and I. P. Williams (2011), Report of the IAU Working Group on Cartographic Coordinates and Rotational Elements: 2009, *Celestial Mechanics and Dynamical Astronomy*, *109*, 101–135, doi:10.1007/s10569-010-9320-4.

Arkani-Hamed, J. (2004), A coherent model of the crustal magnetic field of Mars, *J. Geophys. Res.*, *109*, E09005, doi:10.1029/2004JE002265.

Brain, D. A., F. Bagenal, M. H. Acuña, and J. E. P. Connerney (2003), Martian magnetic morphology: Contributions from the solar wind and crust, *J. Geophys. Res.*, *108*, 1424, doi:10.1029/2002JA009482.

Cain, J. C., B. B. Ferguson, and D. Mozzoni (2003), An n = 90 internal potential function of the Martian crustal magnetic field, *J. Geophys. Res.*, *108*, 5008, doi:10.1029/2000JE001487.

Chamberlain, J. W., and D. M. Hunten (1987), *Theory of Planetary Atmospheres*, 2nd

ed., Academic Press, New York.

Connerney, J. E. P., M. H. Acuna, P. J. Wasilewski, N. F. Ness, H. Reme, C. Mazelle, D. Vignes, R. P. Lin, D. L. Mitchell, and P. A. Cloutier (1999), Magnetic lineations in the ancient crust of Mars, *Science*, *284*, 794, doi:10.1126/science.284.5415.794.

Connerney, J. E. P., M. H. Acuña, P. J. Wasilewski, G. Kletetschka, N. F. Ness, H. Rème, R. P. Lin, and D. L. Mitchell (2001), The global magnetic field of Mars and implications for crustal evolution, *Geophys. Res. Lett.*, *28*, 4015–4018, doi:10.1029/2001GL013619.

Connerney, J. E. P., M. H. Acuña, N. F. Ness, G. Kletetschka, D. L. Mitchell, R. P. Lin, and H. Reme (2005), Tectonic implications of Mars crustal magnetism, *Proceedings of the National Academy of Science*, *102*, 14,970–14,975, doi:10.1073/pnas.0507469102.

Connerney, J. E. P., J. Espley, P. Lawton, S. Murphy, J. Odom, R. Oliversen, and D. Sheppard (2015), The MAVEN Magnetic Field Investigation, *Space Sci. Rev.*, *195*, 257–291, doi:10.1007/s11214-015-0169-4.

England, S. L., G. Liu, P. Withers, E. Yiğit, D. Lo, S. Jain, N. M. Schneider, J. Deighan, W. E. McClintock, P. R. Mahaffy, M. Elrod, M. Benna, and B. M. Jakosky (2016), Simultaneous observations of atmospheric tides from combined in situ and remote observations at Mars from the MAVEN spacecraft, *J. Geophys. Res.*, *121*, 594–607, doi:10.1002/2016JE004997.

Fallows, K., P. Withers, and M. Matta (2015), An observational study of the influence of solar zenith angle on properties of the M1 layer of the Mars ionosphere, *J. Geophys. Res*, *120*, 1299–1310, doi:10.1002/2014JA020750.

Forget, F., F. Montmessin, J.-L. Bertaux, F. González-Galindo, S. Lebonnois, E. Quémerais, A. Reberac, E. Dimarellis, and M. A. López-Valverde (2009), Density and

temperatures of the upper Martian atmosphere measured by stellar occultations with Mars Express SPICAM, *J. Geophys. Res.*, *114*, E01004, doi:10.1029/2008JE003086.

Holstein-Rathlou, C., A. Maue, and P. Withers (2016), Atmospheric studies from the Mars Science Laboratory Entry, Descent and Landing atmospheric structure reconstruction, *Planet. Space Sci.*, *120*, 15–23, doi:10.1016/j.pss.2015.10.015.

Langlais, B., M. E. Purucker, and M. Mandea (2004), Crustal magnetic field of Mars, *J. Geophys. Res.*, *109*, E02008, doi:10.1029/2003JE002048.

Lo, D. Y., R. V. Yelle, N. M. Schneider, S. K. Jain, A. I. F. Stewart, S. L. England, J. I. Deighan, A. Stiepen, J. S. Evans, M. H. Stevens, M. S. Chaffin, M. M. J. Crismani, W. E. McClintock, J. T. Clarke, G. M. Holsclaw, F. Lefèvre, and B. M. Jakosky (2015), Nonmigrating tides in the Martian atmosphere as observed by MAVEN IUVS, *Geophys. Res. Lett.*, *42*, 9057–9063, doi:10.1002/2015GL066268.

Magalhães, J. A., J. T. Schofield, and A. Seiff (1999), Results of the Mars Pathfinder Atmospheric Structure Investigation, *J. Geophys. Res.*, *104*, 8943–8956.

Mahaffy, P. R., M. Benna, T. King, D. N. Harpold, R. Arvey, M. Barciniak, M. Bendt, D. Carrigan, T. Errigo, V. Holmes, C. S. Johnson, J. Kellogg, P. Kimvilakani, M. Lefavor, J. Hengemihle, F. Jaeger, E. Lyness, J. Maurer, A. Melak, F. Noreiga, M. Noriega, K. Patel, B. Prats, E. Raaen, F. Tan, E. Weidner, C. Gundersen, S. Battel, B. P. Block, K. Arnett, R. Miller, C. Cooper, C. Edmonson, and J. T. Nolan (2015), The Neutral Gas and Ion Mass Spectrometer on the Mars Atmosphere and Volatile Evolution mission, *Space Sci. Rev.*, *195*, 49–73, doi:10.1007/s11214-014-0091-1.

McClintock, W. E., N. M. Schneider, G. M. Holsclaw, J. T. Clarke, A. C. Hoskins, I. Stewart, F. Montmessin, R. V. Yelle, and J. Deighan (2015), The Imaging Ultra-

violet Spectrograph (IUVS) for the MAVEN mission, *Space Sci. Rev.*, *195*, 75–124, doi:10.1007/s11214-014-0098-7.

Mendillo, M., S. Smith, J. Wroten, H. Rishbeth, and D. Hinson (2003), Simultaneous ionospheric variability on Earth and Mars, *J. Geophys. Res.*, *108*, 1432, doi:10.1029/2003JA009961.

Montmessin, F., J.-L. Bertaux, E. Quémerais, O. Korablev, P. Rannou, F. Forget, S. Perrier, D. Fussen, S. Lebonnois, A. Rébérac, and E. Dimarellis (2006), Subvisible CO_2 ice clouds detected in the mesosphere of Mars, *Icarus*, *183*, 403–410, doi:10.1016/j.icarus.2006.03.015.

Purucker, M., D. Ravat, H. Frey, C. Voorhies, T. Sabaka, and M. Acuña (2000), An altitude-normalized magnetic map of Mars and its interpretation, *Geophys. Res. Lett.*, *27*, 2449–2452, doi:10.1029/2000GL000072.

Withers, P. (2006), Mars Global Surveyor and Mars Odyssey Accelerometer observations of the Martian upper atmosphere during aerobraking, *Geophys. Res. Lett.*, *33*, L02201, doi:10.1029/2005GL024447.

Withers, P., S. W. Bougher, and G. M. Keating (2003), The effects of topographically-controlled thermal tides in the martian upper atmosphere as seen by the MGS accelerometer, *Icarus*, *164*, 14–32, doi:10.1016/S0019-1035(03)00135-0.

Withers, P., M. Mendillo, D. P. Hinson, and K. Cahoy (2008), Physical characteristics and occurrence rates of meteoric plasma layers detected in the martian ionosphere by the Mars Global Surveyor Radio Science Experiment, *J. Geophys. Res.*, *113*, A12314, doi:10.1029/2008JA013636.

Withers, P., R. Pratt, J.-L. Bertaux, and F. Montmessin (2011), Observations of thermal

tides in the middle atmosphere of Mars by the SPICAM instrument, *J. Geophys. Res.*, *116*, E11005, doi:10.1029/2011JE003847.

Zurek, R. W., R. H. Tolson, D. Baird, M. Z. Johnson, and S. W. Bougher (2015), Application of MAVEN Accelerometer and attitude control data to Mars atmospheric characterization, *Space Sci. Rev.*, *195*, 303–317, doi:10.1007/s11214-014-0095-x.

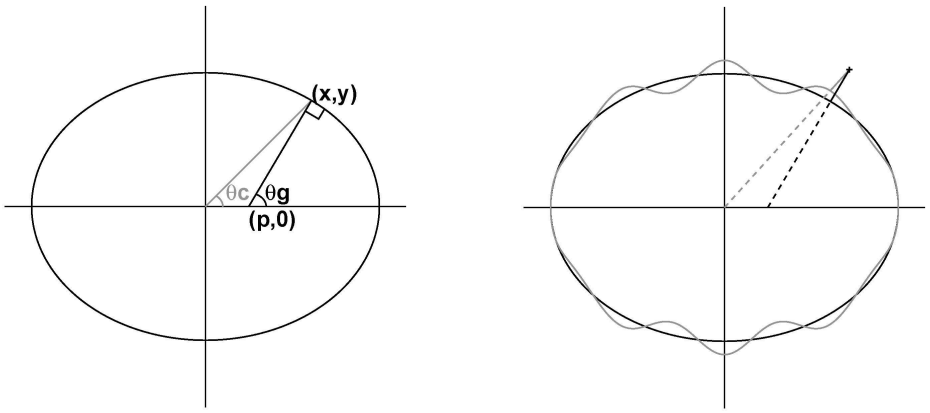

Figure 1. Figure 1A. Illustration of differences between planetographic latitude, θ_g (black), and planetocentric latitude, θ_c (grey). Point (x, y) lies on the planetographic reference ellipsoid. The line from point $(p, 0)$ in the equatorial plane to point (x, y) is perpendicular to the perimeter of the ellipse. Figure 3B. Illustration of differences between planetographic altitude (black) and planetocentric altitude (grey). The black ellipse represents the planetographic reference surface. The straight black line is normal to this reference surface and passes through the point of interest. The straight black line changes from dashed to solid when it crosses the planetographic reference surface. The length of the solid portion of the straight black line illustrates the planetographic altitude. The wavy grey line represents the planetocentric reference surface. The straight grey line joins the origin to the point of interest. The straight grey line changes from dashed to solid when it crosses the planetocentric reference surface. The length of the solid portion of the straight grey line illustrates the planetocentric altitude.

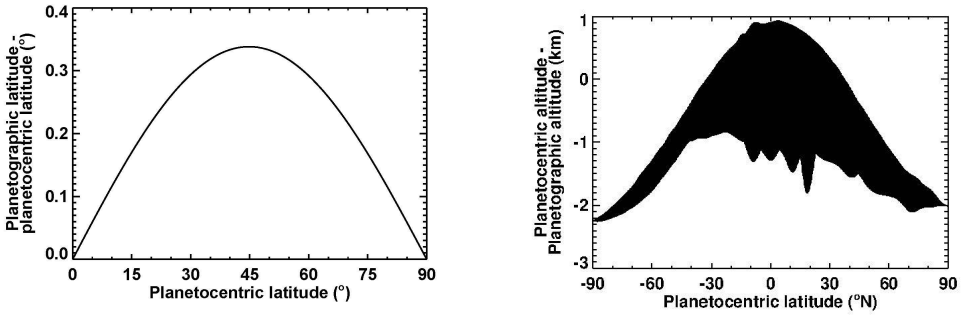

Figure 2. Figure 2A. Difference between planetographic and planetocentric latitudes as function of planetocentric latitude. Figure 2B. Difference between planetocentric altitude and planetographic altitude as function of planetocentric latitude. Since the radius of the planetocentric reference surface varies with longitude, there is a range of values at a given latitude.

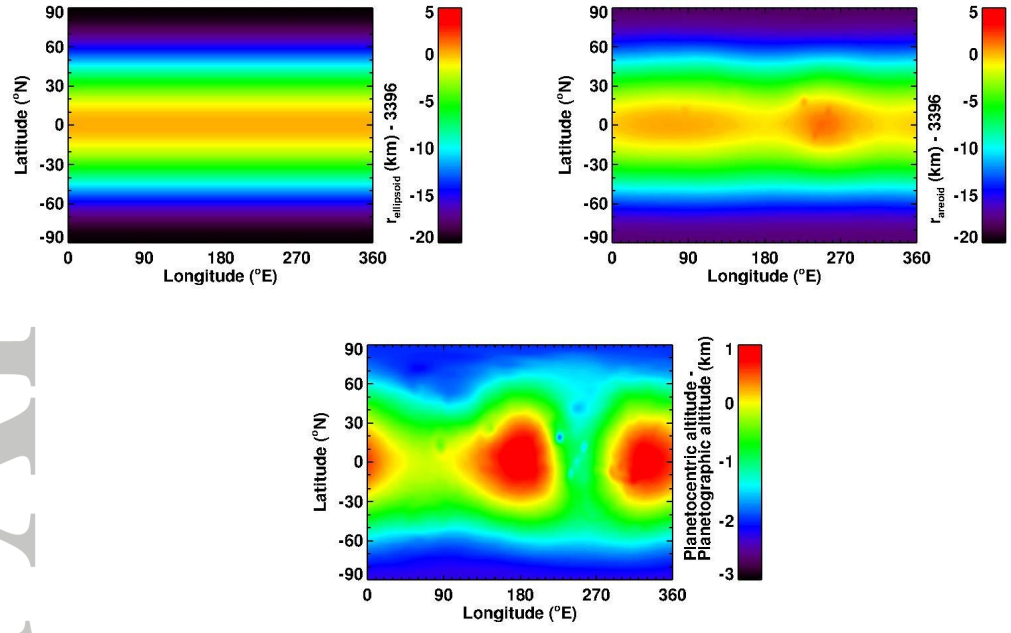

Figure 3. Figure 3A. Radius of planetographic reference surface as function of *planetocentric* latitude and longitude. This reference surface is an ellipsoid of revolution that has no dependence on longitude. Figure 3B. Radius of planetocentric reference surface as function of planetocentric latitude and longitude. Variations with latitude are strongest, but variations with longitude are apparent, particularly in the Tharsis region. Figure 3C. Difference between planetocentric altitude and planetographic altitude as function of planetocentric latitude and longitude. This is equivalent to the difference between the radius of the planetographic reference surface and the radius of the planetocentric reference surface. Variations with latitude are strongest, but variations with longitude are apparent, particularly in the tropics.